Magnetic structures: neutron diffraction studies

1991 Phys. Scr. 44 27

(http://iopscience.iop.org/1402-4896/44/1/002)

Physica Scripta. Vol. 44, 27–32, 1991.

Magnetic Structures: Neutron Diffraction Studies

F. Bourée-Vigneron

Laboratoire Léon Brillouin (CEA-CNRS), CEN-SACLAY, F-91191 GIF-SUR-YVETTE Cedex, France

Received July 13, 1990; accepted November 14, 1990

Abstract

Neutron diffraction is often an unequivocal method for determining magnetic structures. Here we present some typical examples, stressing the sequence through experiments, data analysis, interpretation and modelisation.

Two series of compounds are chosen: (a) RT_2X_2 (R = Rare Earth, T = 3*d* metal and X = Si or Ge), (b) RBe_{13} (R = Rare Earth).

Depending on the nature of the elements R, T, X, the magnetic structures produced can be commensurate, incommensurate or even show a transition between two such phases as a function of temperature.

A model, taking magnetic exchange and anisotropy into account, will be presented in the case of commensurate-incommensurate magnetic transitions in RBe_{13}.

1. Introduction

The only direct method to determine magnetic structures (ferromagnetic or antiferromagnetic, colinear or non-colinear, commensurate or incommensurate . . .) is magnetic neutron diffraction.

The interaction between an atom and a thermal neutron may be accounted for by a scattering amplitude

$$b + 2BI \cdot S + (\gamma r_0/2)M_\perp \cdot S.$$

The first and second term in this expression are of nuclear origin: b is the isotropic nuclear scattering length ($b \sim 10^{-12}$ cm); $2BI \cdot S$ expresses the interaction between the spin of the nucleus I and the spin of the neutron S. In the general case of an unpolarised sample ($\langle I \rangle = 0$), this term gives only rise to incoherent scattering.

The third term $(\gamma r_0/2)M_\perp \cdot S$ corresponds to the dipolar interaction between the magnetic moment of the neutron and the electronic magnetic moment of the atom M (spin and orbital contributions). $M_\perp$ denotes the component of M perpendicular to the scattering vector K: $M_\perp = (K/K) \wedge (M \wedge (K/K))f(K)$ with $f(K)$, magnetic form factor.

Let us notice that the nuclear scattering amplitude b ($\sim 10^{-12}$ cm) and the magnetic scattering amplitude $(\gamma r_0/2)$ $M_\perp \cdot S$ are of the same order of magnitude: when M is in Bohr magnetons units, $(\gamma r_0/2)$ is equal to 0.27×10^{-12} cm. As a consequence, the magnetic scattering can be easily measured with neutrons.

Thermal neutrons display interferences when scattered from ordered condensed matter systems, thus allowing to determine either crystallographic or magnetic structures.

This elastic coherent scattering is accounted for by nuclear and magnetic structure factors:

$$F_N = \sum_i b_i \exp(2i\pi K \cdot r_i)$$

and

$$F_M = 0.27 \times 10^{-12} \sum_i \{[(M_i \cdot K/K)K/K)] - M_i\} \times f_i(K) \exp(2i\pi K \cdot r_i)$$

With a non polarised incident neutron beam, the neutron intensity diffracted at a 2θ angle ($2d_K \sin\theta = \lambda$) is proportional to $F_N^2 + F_M^2$.

The neutron diffraction experiments can be done either on single crystals (four-circles diffractometer) or polycrystalline materials (two-axis diffractometers). Here we shall be concerned with powder diffraction only.

On Fig. 1, the scheme of a two-axis diffractometer is drawn: G4.1 located on a neutron guide beam at the ORPHEE reactor in Saclay. A Position Sensitive Detector is available (800 cells over a 80 degrees $-$ 2θ range); the usual wavelength is 2.438 Å.

In the next paragraphs, we are not going to present a systematic study of all types of systems studied in magnetic neutron diffraction. We will show the different steps of a neutron diffracton magnetic structure determination: experiment, data analysis, magnetic structure determination and modelisation. For this purpose, we have chosen two series of compounds:

(a) RT_2X_2 with R = Rare Earth, T = 3*d* transition metal, X = Si or Ge
(b) RBE_{13} with R = Rare Earth.

2. $TbNi_2Ge_2$

2.1. *Definition*

$TbNi_2Ge_2$ belongs to the RT_2X_2 series of compounds (with R = Rare Earth, T = *nd* transition metal and X = Si or Ge) with the tetragonal $ThCr_2Si_2$-type crystallographic structure (space-group *I*4/*mmm*). Many of these compounds have been magnetically studied over the last ten years [1]. They offer a great variety of magnetic behaviours, as a function of the elements R, T and X. As an indication, Table I gives the results obtained for the R = Tb/T = Mn, Fe, Co, Ni, Cu/X = Si, Ge compounds. All of them, except $TbFe_2Ge_2$, show a long range antiferromagnetic order; for these compounds, the Néel temperature T_N has two distinct orders of magnitude: ~ 500 K if the 3*d* transition metal is magnetic (Mn) or $\leqslant 50$ K if T is non magnetic (Fe, Co, Ni, Cu). Figure 2 gives two magnetic structures in the series: $TbNi_2Si_2$ and $TbCo_2Si_2$.

For $TbNi_2Ge_2$ the only available data have been obtained in a powder neutron diffraction experiment [2]: two magnetic temperatures are given, respectively equal to 16 K and 9 K. The magnetic structures of the compound have not been solved; the authors only indicate that they are incommensurate.

2.2. *Experiment*

Neutron data were collected on a powder sample, at $T =$ 300 K and $T \leqslant 20$ K, with the 3T2 and G4.1 2-axis diffrac-

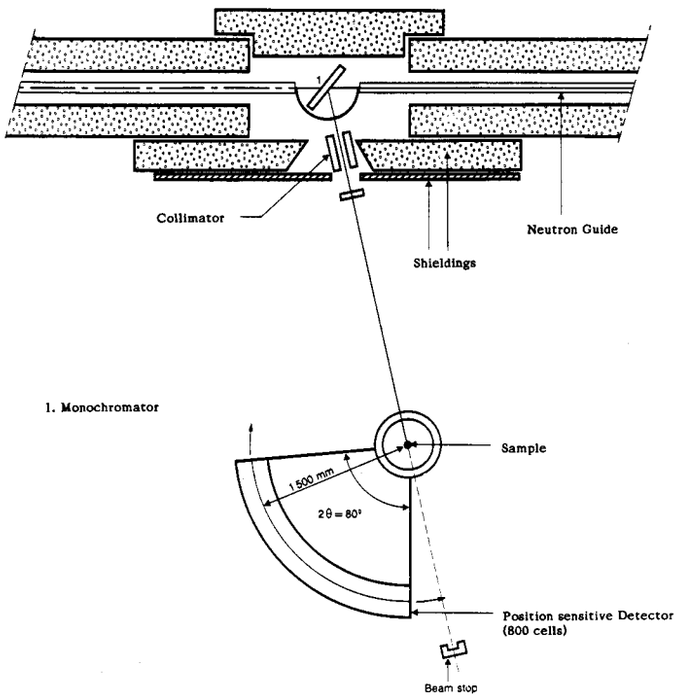

Fig. 1. G4.1 2-axis spectrometer (ORPHEE Reactor, CEN-Saclay).

tometers respectively. The wavelength, angular range and step of the scans were respectively equal to: 1.2263 Å, $6° < 2\theta < 116°$, 0.05° (High Resolution Powder Diffractometer 3T2) and 2.438 Å, $2° < 2\theta < 82°$, 0.10° (G4.1).

2.3. *Data analysis*

The Rietveld [3] profile refinement technique was used for the determination of the crystallographic and magnetic structures. In this procedure a Gaussian profile has been assumed. Two types of parameters are considered:

(1) Those describing the characteristics of the diffractometer: Z (zero position), UVW (Full Width at Half Maximum parameters: $FWHM^2 = U\,\mathrm{tg}^2\theta + V\,\mathrm{tg}\theta + W$) and P (asymmetry parameter).

(2) Those characteristic of the sample: S (overall scale factor), G (preferential orientation parameter), $a\,b\,c\,\alpha\,\beta\,\gamma$ (crystallographic unit cell parameters), $x\,y\,z\,\ldots,n\,\ldots$ (positional parameters and occupation number of the atoms in the nuclear unit cell), $M_x M_y M_z \ldots$ (magnetic moment components) and Debye–Waller factors (either isotropic or anisotropic).

Magnetic structures can be commensurate or incommensurate.

2.3.1. *$T = 300\,K$/Crystalline structure.* The neutron diffraction data at room temperature (3T2) have been analysed within the I4/mmm crystallographic $ThCr_2Si_2$-type structure with Tb in (2*a*) 0.0.0., Ni in (4*d*) 1/2 0. 1/4; 0. 1/2 1/4 and Ge in (4*e*) 0. 0. $\pm z$ ($z \sim 3/8$). The results are given in Table II (the subsequent nuclear scattering amplitudes have been used: $b_{Tb} = 0.738$, $b_{Ni} = 1.030$ and $b_{Ge} = 0.819 \times 10^{-12}$ cm).

2.3.2. *Magnetic structures.* At low temperatures, additional diffraction peaks appear (Figs. 3(a), (b), (c)), which are of magnetic origin and cannot be explained in terms of the tetragonal unit cell. No magnetic contribution is observed at the nuclear Bragg positions.

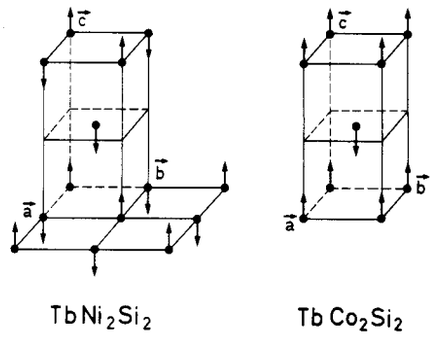

Fig. 2. RT_2X_2. Commensurate magnetic structures of $TbNi_2Si_2$ and $TbCo_2Si_2$.

Table I. *TbT_2X_2 magnetic structures ([1] and references there in). $T_N(K)$ is the magnetic ordering temperature, τ is the propagation vector of the magnetic structure. The direction of the Tb^{3+} magnetic moments is indicated: $\parallel c$ or $\perp c$ (c is the tetragonal crystallographic axis)*

X / *T*	Si	Ge
Mn	$T_N = 550\,K$ Mn {$\tau = (001)$, $M \parallel c$} $T_1 = 65\,K$ Tb^{3+} {F, $M \parallel c$} $T_2 = 55\,K$	$T_N = 415\,K$ Mn {$\tau = (001)$, $M \parallel c$} $T_1 = 110\,K$ Tb^{3+} {F, $M \parallel c$} $T_2 = 25\,K$
Fe	$T_N = 10.5\,K$ $\tau = (0\tau_y\tau_z)$ $M \parallel c$	No long range magnetic order ($T \geqslant 1.8\,K$)
Co	$T_N = 30\,K$ $\tau = (001)$ $M \parallel c$	$T_N = 10.5\,K$ $\tau = (001)$ $M \parallel c$
Ni	$T_N = 10\,K$ $\tau = (\frac{1}{2}\frac{1}{2}0)$ $M \parallel c$	$T_N = 16\,K$; $T_{N'} = 9\,K$
Cu	$T_N = 12\,K$ $\tau = (\frac{1}{2}0\frac{1}{2})$ $M \perp c$	$T_N = 13.5\,K$ $\tau = (\frac{1}{2}0\frac{1}{2})$ $M \perp c$

Table II. *$TbNi_2Ge_2$ crystalline and magnetic parameters*

$TbNi_2Ge_2$	$T = 300\,K$	$T = 12\,K$	$T = 1.45\,K$
2-axis spectrometer	3T2	G4.1	G4.1
Crystalline structure			
a	4.0506(2) Å	4.0362(8) Å	4.0379(16) Å
c	9.7971(4) Å	9.7779(25) Å	9.7824(45) Å
z(Ge)	0.3714(2)	0.3680(12)	0.3696(8)
B_{Tb}	0.285(40)	0	0
B_{Ni}	0.745(25)	0	0
B_{Ge}	0.440(30)	0	0
G	0.195(5)	0.180(45)	0.210(20)
Magnetic structures			
$\tau = \frac{1}{4}c^*$		$M = 8.8(2)\mu_B$	$M = 12.45(35)\mu_B$ $M' = 7.85(30)\mu_B$
$\tau' = \frac{1}{2}(a^* + b^* + c^*)$			$M = 9.50(25)\mu_B$
Reliability factors			
R_N(%)	8.10	9.45	7.55
R_M(%)		5.90	6.05

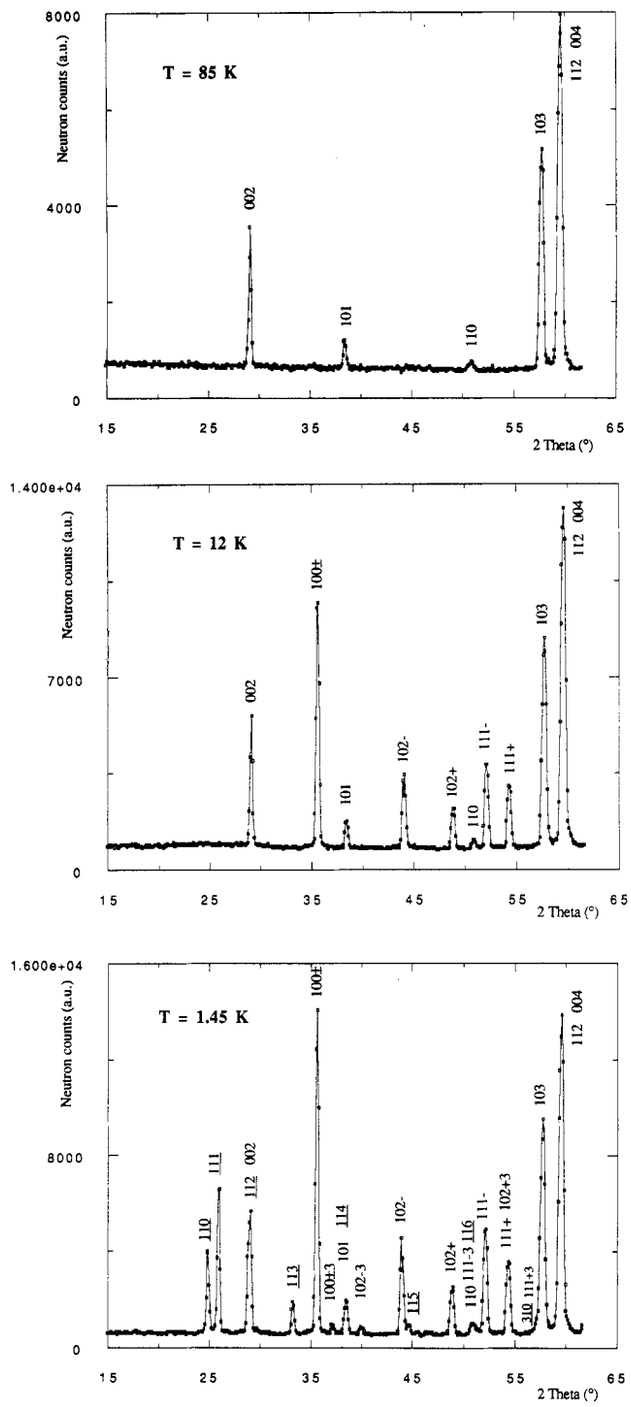

Fig. 3. $TbNi_2Ge_2$ neutron diffraction (λ = 2.438 Å) spectra at (a) T = 85 K ($T > T_N$) (b) T = 12 K ($T_{N'} < T < T_N$) and (c) T = 1.45 K ($T < T_{N'}$). Nuclear Bragg peaks (crystalline unit cell) are labelled hkl. Magnetic Bragg peaks are characteristic of two magnetic unit cells: *aa*4*c* and 2*a*2*a*2*c*; they are respectively labelled hkl^+ . . . (wave vector notation: see Table III) and $\underline{hkl}$.

The first step in a magnetic structure determination is to index these peaks i.e., to determine the magnetic unit cell, or the propagation vector of the magnetic structure.

The additional Bragg peaks observed at T = 12 K (Fig. 3(b)) can be accounted for by a magnetic cell *aa*4*c* i.e., a propagation vector $\tau = 1/4c^*$.

At T = 1.45 K, all the peaks in the diffraction diagram (Fig. 3(c)) cannot be indexed with the only propagation vector $\tau = 1/4c^*$. Another magnetic propagation vector is necessary: $\tau' = 1/2\ (a^* + b^* + c^*)$.

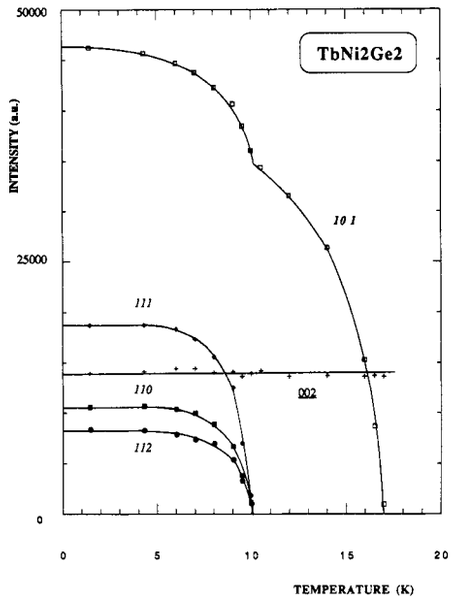

Fig. 4. $TbNi_2Ge_2$ Bragg scattering as a function of T. The ordering temperatures $T_{N'}$ and T_N are deduced from the thermal variation of magnetic intensities 110, 111, 112 (2*a*2*a*2*c* magnetic unit cell; full symbols) and 101 (*aa*4*c* magnetic unit cell; open squares). As a reference, the nuclear Bragg peak 002 (+) is also drawn on the Figure.

A first result, which is obtained in this study, is that the magnetic structures of $TbNi_2Ge_2$ are commensurate, contrary to what is indicated in the literature [2].

Another step in a magnetic neutron diffraction study is to get the value of the magnetic ordering transition temperature(s). To do that, the only way to proceed is to follow the thermal variation of the magnetic intensities. Figure 4 is showing this evolution for the main magnetic Bragg peaks: 110, 111, 112 (magnetic unit cell: 2*a*2*a*2*c*) and 101 (*aa*4*c*). We get T_N = 17 K and $T_{N'}$ = 10.25 K in good agreement with the results of H. Pinto *et al.* [2] (T_N = 16 K and $T_{N'}$ = 9 K).

The last, but not least step, is the study of the magnetic intensities. In the present case, we must distinguish two cases: (1) T = 12 K and (2) T = 1.45 K.

2.3.2.1. T = 12K. The neutron diffraction diagram is obtained in the 2–82° 2θ range but due to Al sample-holder contamination at high 2θ values (111 and 200 Al Bragg peaks) or absence of peaks at low angles, the Rietveld method is only applied from 2θ = 10° to 61.5° (G4.1).

Table III gives the indices of the observed peaks: two conventions are used, either the commensurate magnetic cell *aa*4*c*, either the propagation vector (001/4).

Table III. *$TbNi_2Ge_2$ magnetic Bragg peaks at T = 12 K ($T_{N'} < T < T_N$). Two possibilities exist for indexing the peaks: in the first column, hkl values are indicated in the aa4c magnetic unit cell; in the second column, the same Bragg peaks appear as 1st order satellites ($\tau = 0.25c^*$) of hkl in the nuclear aac cell*

*aa*4*c*	$\tau = \frac{1}{4}c^*$
101	$100^{\pm}$
107	102^{-}
109	102^{+}
113	111^{-}
115	111^{+}

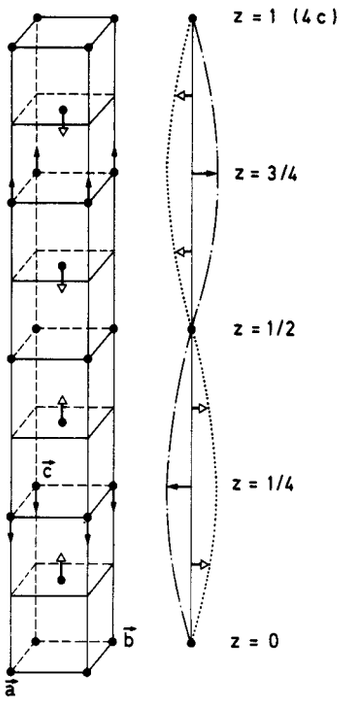

Fig. 5. T = 12 K: $TbNi_2Ge_2$ magnetic structure (longitudinal sine-wave modulation).

We can notice that within the second convention the selection rules are: $hkl^{\pm}$ only with $h+k+l$ odd; no $00l^{\pm}$ peak. These rules correspond to a longitudinal sine-wave modulated structure ($M \| c$) represented on Fig. 5. The analysis of magnetic intensities yields $M = 8.8 \pm 0.2 \mu_B$ at 12 K.

2.3.2.2. T = 1.45 K. The neutron diagram has been obtained in the same experimental conditions as above (T = 12 K). All additional peaks can be accounted for:

(a) either with $\tau = 1/4c^*$: we have $100^{\pm}$, $100^{\pm 3}$, 102^{-3}, 102^{-}, 102^{+}, 111^{-3}, 111^{-}, 111^{+}, 102^{+3}, 111^{+3} i.e., 1st and 3rd order satellites of hkl with $h+k+l$ odd. No $00l^{\pm}$ contribution is observed.

(b) either with $\tau' = 1/2(a^* + b^* + c^*)$. In the magnetic unit cell $2a2a2c$ these peaks are labelled 110, 111, 112, 113, 114, 115, 116 and 310, with h and k satisfying the selection rule h and k odd. This implies that magnetic moments of atoms separated by a (or b) are opposite (cf. Fig. 2 $TbNi_2Si_2$).

The profile analysis of the diagram leads to the moments listed in Table II. All these moments are parallel to the c axis.

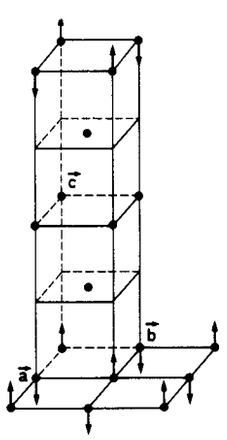

Fig. 6. T = 1.45 K: $TbNi_2Ge_2$ magnetic unit cell $2a2a2c$.

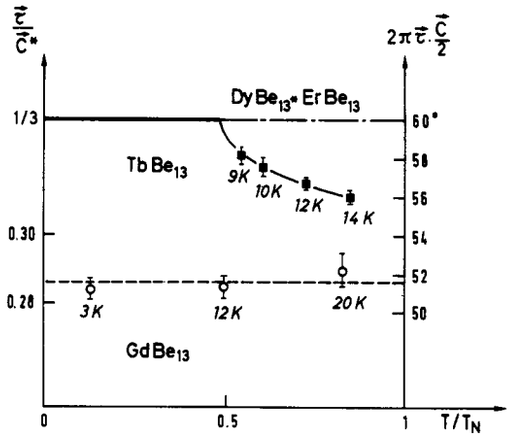

Fig. 7. RBe_{13} magnetic propagation vector τ as a function of T (in reduced units).

The magnetic (001/4) structure looks like that obtained at higher T (12 K) and represented on Fig. 5. The only difference is its squarring up, as revealed by the existence of third order satellites. The ratio of the first and third order components of the magnetic moment (A and B) can be deduced from the ratio M/M': $M = A + B$ and $M' = A - B$, leading to $B/A = 0.225 \sim 2/3\ 1/3$ with $A = 10.15(35)$ and $B = 2.30(35)$. $B/A = 1/3$ would correspond to a perfect squared modulated structure.

The magnetic ($2a2a2c$) structure is given on Fig. 6.

2.4. *Discussion*

Let us notice that the magnetic structure at very low T (T = 1.45 K) as described in the preceding section is not really a reasonable one: for instance, the magnetic moment of Tb^{3+} on $z = 1/4$ ($aa4c$ unit cell) is greater than the saturated Tb^{3+} value: $12.45 = 8.8\sqrt{2} > g_J J = 9\mu_B$. This does not mean that the structure (or profile) refinement is uncorrect, but in the presence case that neutron diffraction cannot yield the relative phases of the two propagating magnetic structures. Some complementary studies are needed to solve the problem, either experimental: magnetic measurements . . . or theoretical: group theory . . .

3. RBe_{13} (R = Gd, Tb, Dy, Ho, Er)

Our intention here is not to give in greater details the neutral diffraction studies on these materials. These can be found in references [4–10]. The results we obtained will only be presented and discussed, as an example of what can be done with neutron diffraction and magnetic structures.

Table IV. *RBe13 magnetic structures. C and I means respectively Commensurate and Incommensurate magnetic structure*

R^{3+}	T_N(K)	$T_{N'}$(K)	Structure
Gd	27 ± 2		I
Tb	16.5 ± 1	8.5	C/I
Dy	10 ± 0.5		C
Ho	6 ± 0.5	4.5	C/I
Er	3 ± 0.25		C

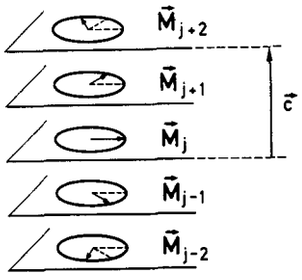

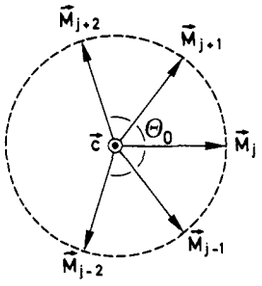

Fig. 8. RBE_{13} incommensurate magnetic structure (helimagnetism).

3.1. *Introduction*

The Rare Earth beryllides RBe_{13} crystallise in the cubic $NaZn_{13}$-type structure, space group *Fm3c* ($a \sim 10$ Å), with 8 R in (a) $\pm[1/4\ 1/4\ 1/4]$, 8 Be in (b) [000]; [1/2 1/2 1/2] and 96 Be in (i) $\pm[0\ y \pm z]$; $\pm[1/2 \pm z\ y]$ with $y \sim 0.114$ and $z \sim 0.176$.

The only magnetic ions in the structure are the R^{3+} ions; they are ordered in a cubic cell of parameter $a/2$. The local symmetry of the R^{3+} site is cubic (43), with a nearly spherical environment, thus leading to a rather small Crystalline Electric Field (CEF overall splitting less than 40 K in the studied series [5]).

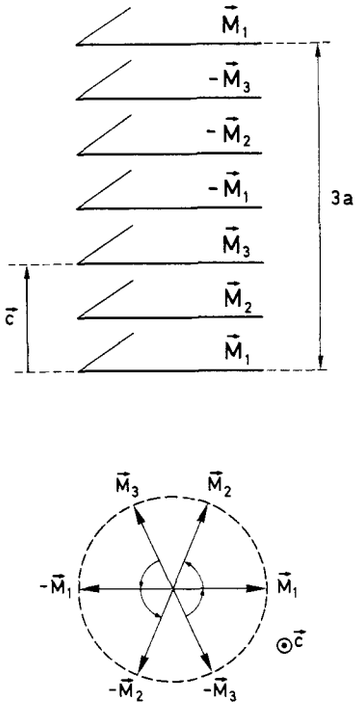

Fig. 9. RBe_{13} commensurate magnetic structure.

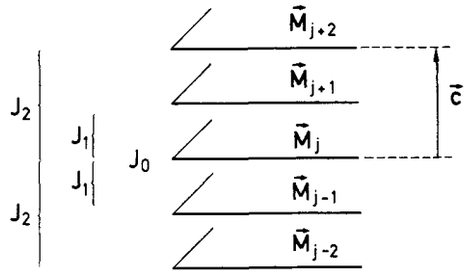

Fig. 10. RBe_{13} magnetic structures: ferromagnetic (001) planes and exchange constants J_0, J_1 and J_2.

The magnetic structures thus result from the competition between exchange and anisotropy, two energy terms which are of the same order of magnitude.

3.2. *Magnetic structures*

Commensurate and/or Incommensurate (spiral) magnetic structures are observed, depending on the nature of the Rare Earth (see Table IV). Figure 7 gives the thermal variation of the propagation vector τ: $\tau = 1/3[1 - \varepsilon(T)]c^*$. Figures 8 and 9 show respectively the incommensurate [$\varepsilon(T) \neq 0$] and commensurate [$\varepsilon(T) = 0$] RBe_{13} magnetic structures.

The commensurate structure, depicted in Fig. 9, is not a regular helimagnetic structure: the sequence of magnetic moments $\boldsymbol{M}_1$, $\boldsymbol{M}_2$, $\boldsymbol{M}_3$ . . . in a regular helix would be $0, \pi/3, 2\pi/3$ . . . and correspond only to 1st order satellites of the nuclear Bragg peaks *hkl*. Here we have $0, \pi/3 + \delta$, $2\pi/3 - \delta$ . . . As an experimental evidence of $\delta \neq 0$, the 3rd order satellites of *hkl* (*h*, *k*, and *l* even) are observed.

3.3. *Model*

As already mentioned, these structures result from a competition of isotropic magnetic exchange and magnetocrystalline anisotropy.

Magnetic exchange is of RKKY type: the Néel temperatures T_N are a function of the de Gennes' parameter $\zeta = (g_J - 1)^2 J(J + 1)$ where $J = L + S$ and g_J is the Landé factor. We have $T_N = \zeta^{1.2}$.

This magnetic exchange can be treated within a molecular field approximation. We define the exchange parameters $J_0 J_1 J_2$ as magnetic interaction between a R^{3+} ion and all the R^{3+} ions in the same ferromagnetic (001) plane, in the nearest and next-nearest (001) planes respectively (Fig. 10).

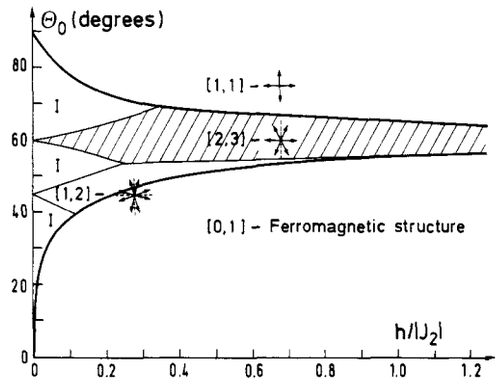

Fig. 11. RBe_{13} magnetic phase diagram (*x*-axis = anisotropy, *y*-axis = exchange). I means Incommensurate (regular helix); the Commensurate Magnetic Structures are labelled [*p*, *q*] and drawn in the corresponding areas of the diagram.

The exchange energy is then written as:

$$H_{\text{Exchange}} = -J_0 - J_1\langle\cos(\theta_{j+1} - \theta_j)\rangle - J_2\langle\cos(\theta_{j+2} - \theta_j)\rangle$$

where θ_j is the angle between one easy magnetisation axis and the magnetic moments M_j in the ferromagnetic (001) jth plane.

For $GdBe_{13}$, this term is the only energy term: Gd^{3+} is an S ion, with no magnetocrystalline anisotropy. An incommensurate helimagnetic structure is easily obtained when $J_0 > 0$, $J_1 > 0$, $J_2 < 0$ and $J_1 + 4J_2 < 0$: the regular angle θ_0 between two magnetic moments in nearest (001) planes is then $\cos\theta_0 = -J_1/4J_2$.

For RBe_{13}, with R = Tb, Dy, Ho, Er, anisotropy corresponds to an easy (001) plane; within this plane easy magnetisation axis are perpendicular. We can write:

$$H_{\text{Anistropy}} = -h\langle\cos n\theta_j\rangle$$

with $n = 4$ in the present case (tetragonal symmetry).

We must look for a minimum of $H = H_{\text{Exchange}} + H_{\text{Anisotropy}}$ with $H = -4\cos\theta_0\langle\cos(\theta_{j+1} - \theta_j)\rangle + \langle\cos(\theta_{j+2} - \theta_j)\rangle - h\langle\cos 4\theta_j\rangle$.

The solution we try is $\theta_j = j\theta + \alpha + A\sin 4(j\theta + \alpha)$, with parameters θ, α and A.

In the expression of H two cases must be distinguished for the mean values determination: incommensurate and commensurate θ values [$\theta = 2\pi/4 \cdot p/q$ with p and q mutual primes, in the commensurate case].

Two distinct expressions of H are then obtained:

$$H_{\text{INC}} = -4\cos\theta_0 \cdot \cos\theta J_0(z_1) + \cos(2\theta)J_0(z_2) + hJ_1(4A)$$

an expression which, as expected, is α independent.

$H_{p,q}$(commensurate) includes higher order ($k > 1$) Bessel functions $J_k(z)$ of the parameters $z_1 = 2A\sin 2\theta$, $z_2 = 2A\sin 4\theta$, $4A$ and is α dependent.

A numerical minimisation is done for either the incommensurate or the commensurate structure. The "minimum minimorum" is then taken and leads to the magnetic phase diagram of Fig. 11 (x-axis: anistropy, y-axis: exchange). Let us notice that in the commensurate solution the α phase is fixed: $\alpha = 0$ if q odd and $\alpha = \pi/q$ if q even. The commensurate structures [p, q] are also represented on that Figure: the hatched region is that corresponding to the observed commensurate structure in the RBe_{13} series we study.

This type of diagram can interpret (at least in a qualitative way) the thermal variation of the magnetic structure: we can easily imagine that exchange is a constant, but anisotropy is varying with T, increasing when T is lowered. For a given exchange parameters set (J_1, J_2), depending on the initial (i.e., $T > T_N$) value of anisotropy, we can then observe when T is decreased, either a transition from an incommensurate to a commensurate magnetic structure, either an "always" commensurate structure (with A function of T).

4. Conclusion

The preceeding studies on rare earth intermetallics are characteristic examples of magnetic neutron diffraction.

$TbNi_2Ge_2$ exhibits two magnetic transitions as a function of T: below $T_N = 17$ K, the magnetic structure is a longitudinal sine-modulated structure (wave-vector $\tau = 1/4c^*$ and Tb^{3+} magnetic moments $\| c$); below T_N, the Tb^{3+} magnetic moments are still directed along the tetragonal c axis, but at the present time, we have not yet solved the structure completely. Two wave-vectors coexist $\tau = 1/4c^*$ and $\tau' = 1/2(a^* + b^* + c^*)$ and the problem is to determine the relative phases of the two propagating magnetic components.

The neutron diffraction RBe_{13} study is more complete: from experiment to structure determination (commensurate and/or incommensurate magnetic structures) and interpretation (model of competing magnetic exchange and anisotropy). This series of intermetallic compounds has also been studied by other techniques: magnetic measurements, specific heat experiments, Mössbauer effect as a complement to elastic and inelastic neutron scattering [4–10 and references therein].

Finally, as already mentioned, we didn't present in this paper a systematic review of magnetic neutron diffraction: in particular, single crystal studies, polarised neutrons experiments and nuclear magnetic scattering have not been investigated.

Acknowledgments

The author is greatly indebted to A. Olès (Cracovie), P. Mériel, M. Bonnet and P. Becker for their cooperation to the present work.

References

1. Szytula, R. and Leciejewicz, J., Handbook on the Physics and Chemistry of Rare Earths (Eds. K. A. Gschneidner, Jr. and L. Eyring), Vol. 12, ch. 83, Elsevier Science Publishers (1989).
2. Pinto, H., Melamud, M., Kuznietz, M. and Shaked, H., Phys. Rev. **B31**, 508 (1985).
3. Rietveld, H. M., J. Appl. Cryst. **2**, 65 (1969).
4. Vigneron, F., Sougi, M., Meriel, P., Herr, A. and Meyer, A., J. Phys. France **41**, 123 (1980).
5. Vigneron, F., Bonnet, M. and Kahn, R., Crystalline Electric Field and Structural Effects in f-electrons Systems (Edited by J. E. Crow, R. P. Guertin and T. W. Mihalisin) Plenum Publishing Corporation, New York, (1980).
6. Vigneron, F., Bonnet, M., Herr, A. and Schweizer, J., J. Phys. F. **12**, 223 (1982).
7. Vigneron, F., Bonnet, M. and Chappert, J., J. Phys. F. **15**, 181 (1985).
8. Vigneron, F., Bonnet, M., and Becker, P., Physica **130B**, 366 (1985).
9. Becker, P., Bonnet, M. and Vigneron, F., Mol. Cryst. and Liq. Cryst. **125**, 405 (1985).
10. Vigneron, F., Chemica Scripta **26A**, 93 (1986).